Matching and funneling light at the plasmonic Brewster angle

Christos Argyropoulos,[1] Giuseppe D'Aguanno,[2,3] Nadia Mattiucci,[2,3] Neset Akozbek,[2,3] Mark J. Bloemer,[3] and Andrea Alù[1,*]

[1]*Department of ECE, University of Texas at Austin, Austin, Texas 78712, USA*

[2]*AEgis Technologies, Nanogenesis Division, Huntsville, Alabama 35806, USA*

[3]*Department of the Army, Charles M. Bowden Facility, Redstone Arsenal, Alabama 35898, USA*

(Received 7 December 2011; revised manuscript received 10 January 2012; published 31 January 2012)

The ultrabroadband impedance matching of metallic gratings at the plasmonic Brewster angle [A. Alù *et al.*, Phys. Rev. Lett. **106**, 123902 (2011)] is analyzed here in several realistic scenarios and configurations, and in the case of nonmonochromatic excitation. This phenomenon is the analogy of the well-known Brewster transmission for dielectric slabs but, when applied to plasmonic gratings, has the remarkable property of funneling and concentrating light within subwavelength slits. We analyze here how the presence of absorption and of realistic substrates and/or superstrates may influence the phenomenon, its beamwidth and angular selectivity, and its overall performance in the case of broadband, ultrashort incident pulses in the time domain. We prove that broadband signals may be concentrated and transmitted almost unaffected through narrow apertures, even in the presence of absorption, very different from conventional extraordinary optical transmission based on resonant phenomena.

DOI: 10.1103/PhysRevB.85.024304 PACS number(s): 71.45.Gm, 41.20.Jb, 42.25.Ja, 42.79.Dj

I. INTRODUCTION

Extraordinary optical transmission (EOT) through subwavelength apertures in metallic screens has been widely investigated in the past several years.[1–3] Based on several available techniques, the transmission of optical energy through otherwise opaque metallic screens can be drastically enhanced, especially for subwavelength apertures and larger periods. This phenomenon is typically based on resonant mechanisms, such as Fabry-Perot (FP) resonances[1–3] and plasmonic surface resonances, or "spoof plasmons."[4,5] The aforementioned effects are inherently narrow band in nature and are severely affected by the inherent losses of metals at optical frequencies, which may limit their potential applications. For example, EOT based on surface plasmons is usually limited to a narrow frequency range that depends on the properties of the screen material, the slit periodicity, and the background material. More narrow-band performance is found for smaller apertures and thicker screens, characterized by larger stored energy and higher Q-factor resonances. Usually these EOT effects are weakly dependent on the incidence angle, as long as the period of the grating is less than the first Bragg resonance.[6–10]

In our recent work,[11] we proposed an alternative mechanism to achieve extraordinary transmission through an otherwise opaque metallic grating. The phenomenon is the analogy of the well-known Brewster total transmission effect at a vacuum-dielectric interface, which was shown to also work in the case of plasmonic gratings. Different from conventional EOT, this phenomenon is inherently broadband, robust to the presence of loss and absorption, and independent of the screen total thickness. It is limited to transverse-magnetic (TM) polarized electromagnetic waves and allows only a limited portion of the angular spectrum to tunnel through the slits, around the plasmonic Brewster condition derived in Ref. 11. In our original paper, we limited our analysis to a freestanding grating with empty slits. This concept, independently verified in the infrared,[5] has renewed the interest in funneling broadband light for energy-harvesting applications[12] and in related concepts, such as the plasmonic critical angle.[13]

Especially in the optical regime, it is challenging to fabricate a freestanding metal grating[14] and, as we discuss in the following, this concept may be applied to different geometries. Here, we explore several practical scenarios in which the plasmonic Brewster concept may be applied. First, we analyze the case of a single interface between free space and a semi-infinite grating loaded with different dielectric materials. This case is particularly exciting because it may model the application of the plasmonic Brewster phenomenon for energy-harvesting concepts. Once the energy is funneled within subwavelength slits with no reflection, one may expect that light concentration may facilitate its conversion to other forms of energy, without perturbing the low reflection properties. We show that this is the case, and that we are able to achieve broadband funneling of light at a single interface around the Brewster condition, without the presence of a second interface, which is obviously necessary for conventional EOT resonant mechanisms. Then, we explore how the presence of a superstrate and/or substrate with different indices of refraction, as well as different dielectric fillings in the slits, affect the Brewster condition, and find that not only do they not severely impair its performance, but they can add degrees of freedom for the practical application of this phenomenon. The considered examples pave the way to the experimental verification of these concepts at visible frequencies, for which the presence of a substrate and/or superstrate may be required. We are currently working on some of these venues. Then, the effective medium approach, first presented in Ref. 11, is extended and compared with theory and simulation results, including the guided spectrum of modes supported by the grating. Finally, we analyze in detail the transmission of short, broadband pulses through the grating, showing that at the Brewster condition they can be funneled and propagate almost unaffected through ultranarrow slits. These results directly demonstrate and emphasize the ultrabroadband performance of the suggested concept. Novel devices are envisioned from the proposed broadband optical transmission, such as light-emitting diodes, selective polarization filters, and energy concentrators.

II. FREQUENCY-DOMAIN ANALYSIS OF PLASMONIC BREWSTER DEVICES

The general geometry that we consider in the following examples is shown in Fig. 1. It is composed of a silver (Ag) metallic screen (light gray color) of thickness l, corrugated by slits of width w and period d. The slits are loaded with a dielectric material with relative permittivity ε_w (light green color) and the grating is surrounded by a semi-infinite input (ε_{in}) and output (ε_{out}) medium, shown in Fig. 1 with light yellow and light red colors, respectively. In practice, we may need a double prism configuration to efficiently couple light in and out of this setup in the presence of arbitrary superstrate and substrate materials. Figure 1 can be considered the generalized version of the setup studied in Ref. 11. The structure is illuminated by a TM wave obliquely incident at an angle θ. The scattering performance of such a periodic structure may be modeled using a transmission-line (TL) approach, as described in Refs. 11,15 and 16. The circuit model of this structure is also shown in Fig. 1, where input and output regions correspond to semi-infinite TLs and the grating region (light gray color) is a TL segment of length l.

For a TM wave incident at an angle θ, the effective wave number of the input medium is the projection of the wave vector in the direction normal to the interface, i.e., $\beta_{\text{in}} = k_{\text{in}} \cos\theta$, where $k_{\text{in}} = n_{\text{in}} k_0$ and $n_{\text{in}} = \sqrt{\varepsilon_{\text{in}}}$ is the refractive index. The characteristic impedance of the input medium per unit length is then given by the ratio between the tangential electric and magnetic fields with respect to the interface, normalized to the grating period:

$$Z_{\text{in}} = \sqrt{\frac{\mu_0}{\varepsilon_{\text{in}}\varepsilon_0}}\, d\, \cos(\theta) = \frac{\eta_0}{n_{\text{in}}}\, d\, \cos(\theta), \tag{1}$$

computed in the same way as in Refs. 11 and 15, and $\eta_0 = \sqrt{\mu_0/\varepsilon_0}$ is the vacuum impedance. The characteristic impedance per unit length of the output medium may be similarly calculated using momentum conservation:

$$Z_{\text{out}} = \sqrt{\frac{\mu_0}{\varepsilon_{\text{out}}\varepsilon_0}}\, d \sqrt{1 - \frac{\sin^2(\theta)}{\varepsilon_{\text{out}}}} = \frac{\eta_0}{n_{\text{out}}}\, d \sqrt{1 - \frac{\sin^2(\theta)}{n_{\text{out}}^2}}. \tag{2}$$

The modal propagation inside each slit does not depend on the incidence angle. The wave number β_s and characteristic impedance per unit length Z_s satisfy the modal dispersion equations in a metal-insulator-metal (MIM) plasmonic waveguide:[17]

$$\tanh\left[\sqrt{\beta_s^2 - \varepsilon_w k_0^2}\, w/2\right] \sqrt{\beta_s^2 - \varepsilon_w k_0^2} = -\frac{\varepsilon_w}{\varepsilon_m} \sqrt{\beta_s^2 - k_0^2 \varepsilon_m},$$
$$Z_s = w\beta_s/(\omega\varepsilon_0\varepsilon_w), \tag{3}$$

where ε_m is the relative permittivity of the metal (considered to be Ag here) and Z_s is the ratio between the effective voltage $V_s = \int_0^w E_x\, dx = E_x w$ and the effective current $I_s = H_y = \omega\varepsilon_0\varepsilon_w E_x/\beta_s$. Frequency dispersion and absorption of Ag are considered in Eq. (3), and determine the modal properties and spatial decay within each slit of the dominant TM mode. The dielectric materials used as superstrate/substrate and/or to fill the slits are assumed frequency independent in the following. This simple TL model applies to TM incidence for monomodal operation inside the slits and it assumes that only the zeroth diffraction order propagates in free space, implying that the dimensions are limited to the range $w \ll d < 0.5\lambda_0 = \pi/k_0$, where λ_0 can be the wavelength at free space or the substrate/superstrate. We verify in the following that this simple analytical model captures with good accuracy the main phenomena at the basis of the plasmonic Brewster matching phenomenon, and more in general of the wave interaction with the grating.

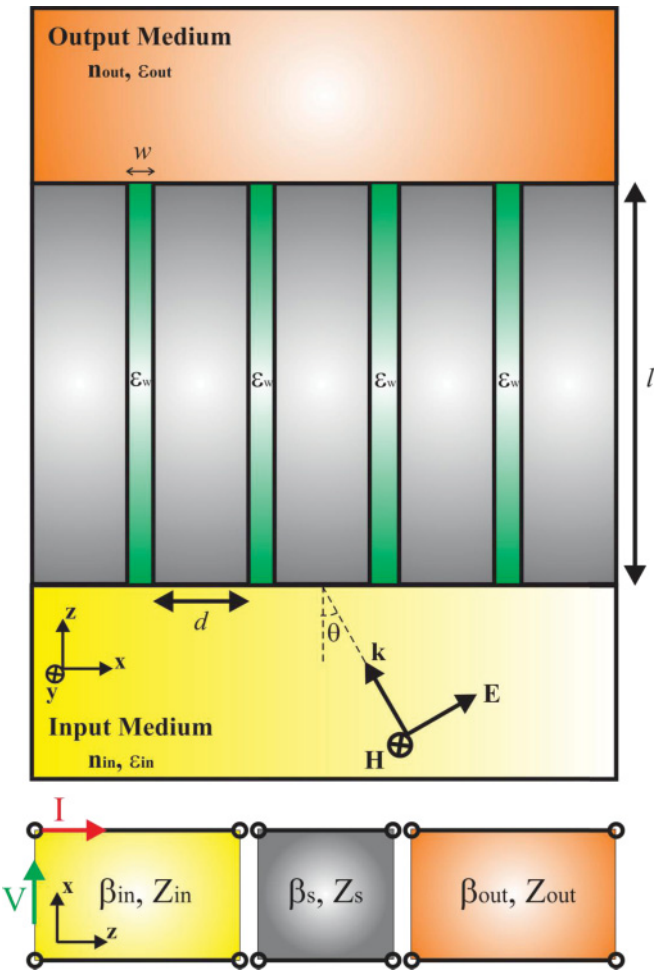

FIG. 1. (Color online) Geometry of interest and its equivalent transmission-line (TL) model.

A. Semi-infinite grating

We consider first the case of the interface between free space ($n_{\text{in}} = 1$) and a semi-infinite grating, obtained in the limit $l \to \infty$ for the geometry of Fig. 1. The reflection and transmission coefficients at the grating entrance may be computed using the TL model, providing the usual Fresnel expressions:

$$R = \frac{Z_s - Z_{\text{in}}}{Z_s + Z_{\text{in}}},$$
$$T = \frac{2Z_{\text{in}}}{Z_s + Z_{\text{in}}}. \tag{4}$$

These expressions predict that a nonresonant, Brewster-like effect based on anomalous impedance matching may also be obtained in the absence of an external interface, which was the case studied in Ref. 11. In this scenario, no other EOT

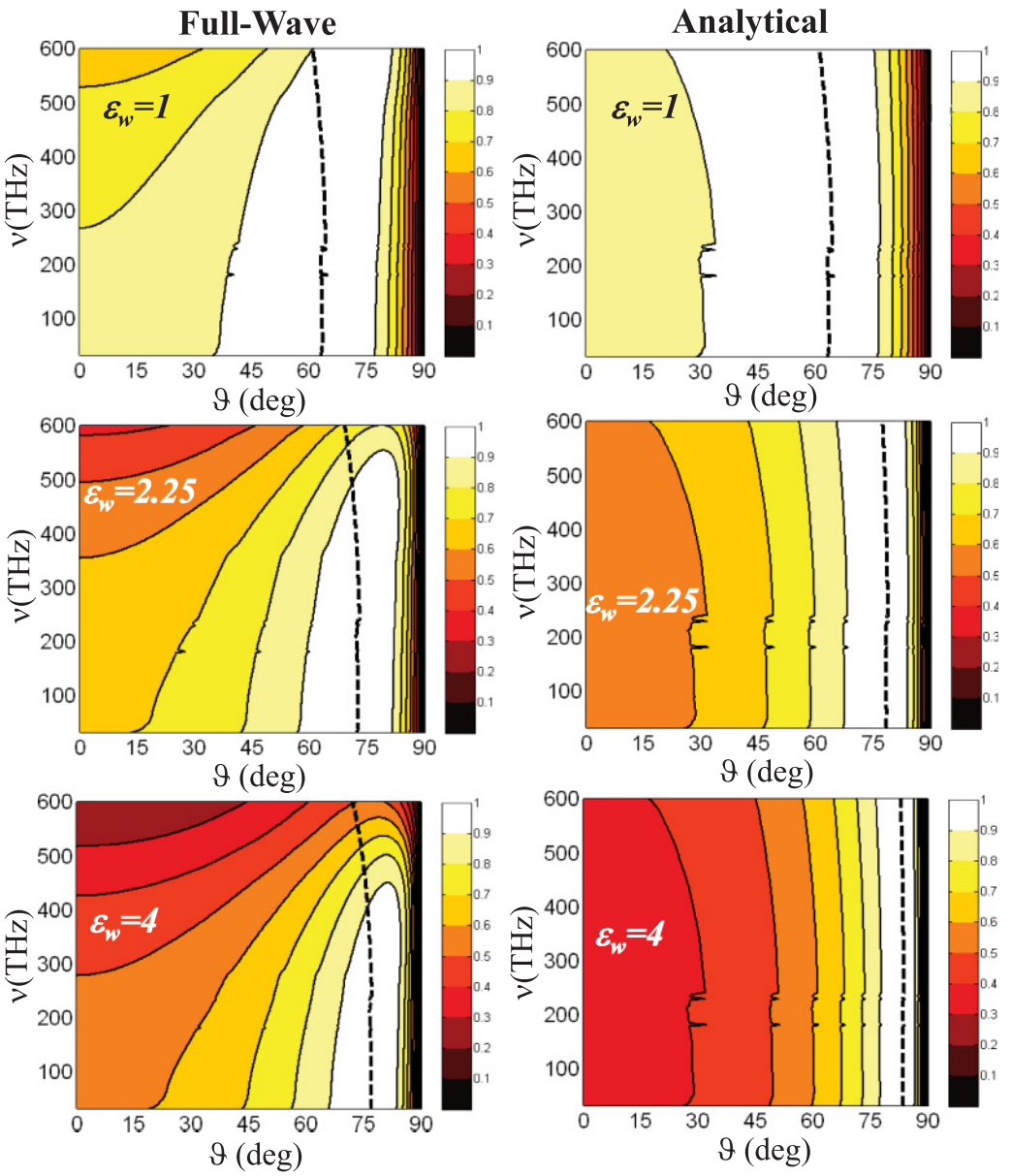

FIG. 2. (Color online) Angular transmission spectra for a single interface between free space and a grating with period $d = 96$ nm and slit width $w = 24$ nm. Different permittivity values ε_w are considered inside the slits, as indicated in each panel. FMM simulations (left) are compared with analytical results (right). The dashed line indicates the plasmonic Brewster angle condition (5).

mechanism is available, such as conventional Fabry-Perot resonant tunneling (see Ref. 2), which would require a finite slab thickness and multiple reflections. When the grating impedance is matched to the input medium ($Z_s = Z_{\text{in}}$), total tunneling through the slits ($T = 1$) and zero reflection is achieved. For free space as input medium, the matching condition may be realized at the angle of incidence θ_B such that

$$\cos\theta_B = \frac{\beta_s w}{\varepsilon_w k_0 d}, \tag{5}$$

which coincides with the plasmonic Brewster angle condition derived in Ref. 11, generalized here to an arbitrary dielectric in the slits and holding also for a single interface. The free-space input impedance, generally larger than the one in the slit due to the large value of d/w, is reduced for oblique incidence and TM polarization, providing ideal matching when Eq. (5) is satisfied.

The Brewster condition is weakly dependent on frequency (it is only affected by the dispersion of β_s/k_0) and not sensibly affected by moderate losses, as long as $\text{Re}[\beta_s] \gg \text{Im}[\beta_s]$, as is usually the case for plasmonic MIM waveguides over a broad range of frequencies. We notice from Eq. (5) that the plasmonic Brewster angle shifts to larger values (closer to grazing) as the slit permittivity ε_w is increased.

In Fig. 2, we calculate the TM power transmission spectra for such interface, considering a period $d = 96$ nm and slit width $w = 24$ nm. The permittivity ε_w of the slit material is indicated in each panel. The left column shows full-wave simulations based on the Fourier modal method (FMM),[18]

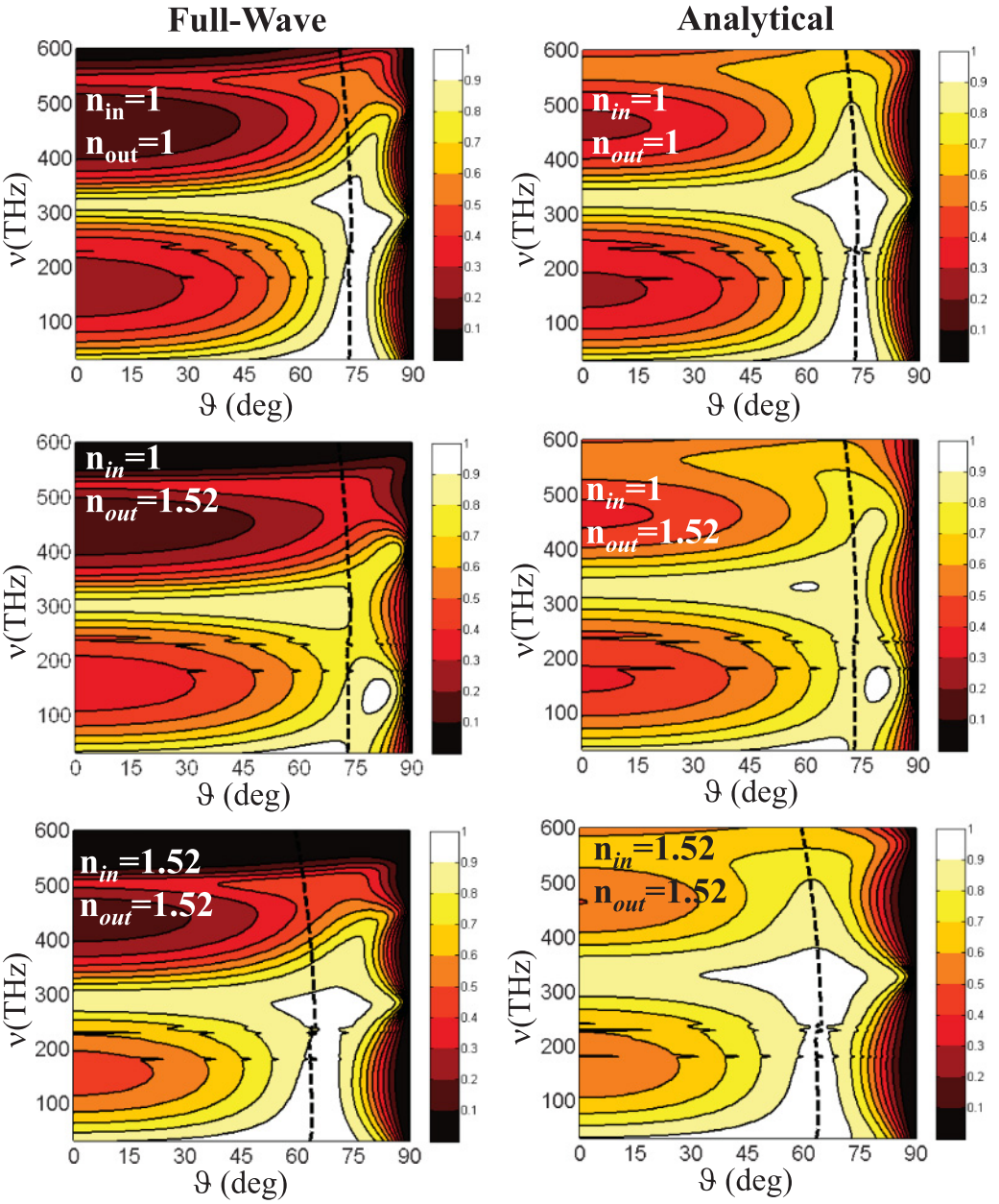

FIG. 3. (Color online) Angular transmission spectra for a grating with thickness $l = 200$ nm, period $d = 96$ nm, and slit width $w = 12$ nm. The refractive indices of the input and output media are indicated in each panel. FMM simulations (left) are compared with analytical results (right). Again, the dashed line indicates the plasmonic Brewster angle condition. The material between the slits of the structure is chosen to be free space $\varepsilon_w = 1$.

compared to our analytical TL model (right column). Realistic experimental dispersion and loss of silver permittivity at optical frequencies[19] are considered here and in the following. The TL model is in very good agreement with full-wave simulations and confirms that Eq. (5) is an accurate tool to predict the Brewster matching condition and model this geometry. The plasmonic Brewster tunneling is found as a vertical band in all panels in Fig. 2, confirming the weak dependence on frequency of this anomalous funneling mechanism. As expected, full transmission is achieved only around the Brewster angle condition, predicted in Eq. (5) and highlighted as the dashed line in each panel. Comparing these results with the ones obtained in the case of a finite l (see Ref. 11 and some of the following examples), it is seen that all the resonant horizontal EOT bands in the figure are suppressed, since conventional Fabry-Perot resonances require an exit interface to build the resonance in the steady-state regime.

The transmission maxima are reduced for higher frequencies, due to the influence of larger absorption in the slit. In this frequency range, the influence of higher diffraction orders slightly affects the accuracy of our analytical model. It is evident that the vertical bands of Brewster transmission are strongly influenced by the slit material, as theoretically

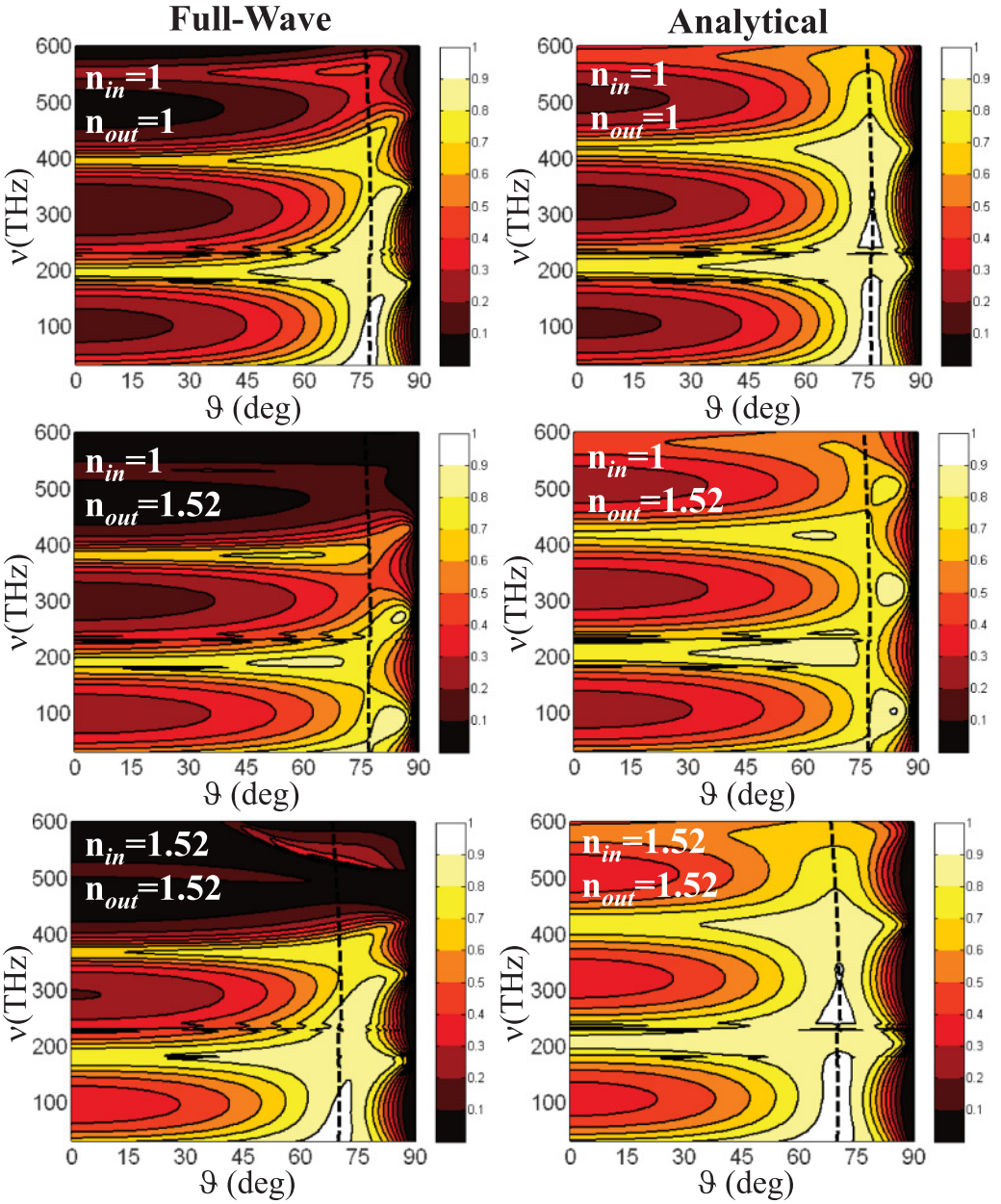

FIG. 4. (Color online) Similar to Fig. 3, but for thicker screens and a larger period: $l = 400$ nm and $d = 192$ nm. The slit width is chosen as $w = 24$ nm.

predicted in Eq. (5). In addition to a shift to more grazing angles, an increase in the slit permittivity produces narrower acceptance beamwidths, due to larger impedance mismatch, consistent with the impedance model (1): Z_{in} is further reduced by increasing ε_{in}, requiring a more grazing incidence angle to match the free-space impedance. Note that the same effect will also be observed for larger ratios of slit width over grating period (w/d). This can lead to novel designs of more directional emitters and angle-sensitive absorbers or solar cells, as will be explored in our future work. All the aforementioned effects are accurately predicted with both FMM simulations and the TL model. Indeed, our results show that it is possible to funnel broadband light into subwavelength grating at a single interface, with exciting implications in terms of energy harvesting.

B. Influence of superstrate and/or substrate materials

After having verified that a single interface already supports Brewster transmission and funneling, we focus here on the case of finite thickness gratings, as in Fig. 1. The general input Z_{in} and output Z_{out} characteristic impedances are given by Eqs. (1) and (2). The loading material of the slits is assumed to be free-space $\varepsilon_w = 1$ here. The reflection and transmission coefficients of the finite grating may be written as

$$R = \frac{\left(Z_s^2 - Z_{\text{in}}Z_{\text{out}}\right)\tan(\beta_s l) - i(Z_{\text{in}} - Z_{\text{out}})Z_s}{\left(Z_s^2 + Z_{\text{in}}Z_{\text{out}}\right)\tan(\beta_s l) + i(Z_{\text{in}} + Z_{\text{out}})Z_s},$$
$$T = \frac{2Z_{\text{out}}Z_s\ \sec(\beta_s l)}{(Z_{\text{in}} + Z_{\text{out}})Z_s + i\left(Z_s^2 + Z_{\text{in}}Z_{\text{out}}\right)\tan(\beta_s l)}. \quad (6)$$

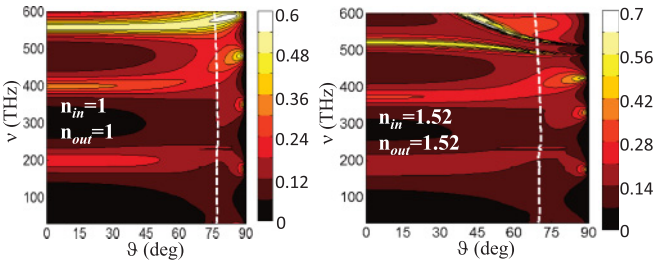

FIG. 5. (Color online) Calculated absorption for two examples consistent with Fig. 4.

As expected, if the input and output media are also free space, the reflection coefficient of Eqs. (6) becomes identical to the one calculated in Ref. 11. The real part of the reflection coefficient is zero, $\mathrm{Re}[R] = 0$, when the condition $\beta_s l = m\pi$ is met, where m is an integer. FP resonances are obtained in this case, which are the conventional EOT mechanism for this geometry,[1] inherently limited in bandwidth. The minimum reflection is, however, limited by the mismatch between input and output materials, which affects $\mathrm{Im}[R]$. As a different way to achieve minimized reflection, impedance matching analogous to the previous example may be achieved at the input interface when $Z_s = Z_{\mathrm{in}}$, under the condition

$$\cos\theta_B = \frac{n_{\mathrm{in}}\beta_s w}{k_0 d}. \tag{7}$$

This is equivalent to Eq. (5), but now considering a different superstrate material at the input face of the grating and free space in the slits. As expected, the plasmonic Brewster angle is independent of the grating thickness l, and similar considerations apply as in the previous section. Now the plasmonic Brewster angle is inversely proportional to the dielectric function of the superstrate material, implying that we can shift the funneling to smaller angles by using higher permittivity superstrates.

The calculated angular power transmission spectra are shown in Fig. 3 for an optical grating with length $l = 200$ nm, period $d = 96$ nm, and slit width $w = 12$ nm. The dielectric functions of the input and output background media are varied as indicated in each panel. Again, the left column shows full-wave simulations based on the FMM,[18] compared to the analytical TL model shown in the right column, which shows good agreement in all cases. The FP resonances are now visible as horizontal bands in all panels of Fig. 3, limited in frequency, but spanning most of the angular spectrum.

In contrast, the plasmonic Brewster transmission results in a distinct vertical band through all panels in Fig. 3. Glass is used as an input and/or output background medium, with a refractive index $n = 1.52$. The dashed line in the plots shows the calculated Brewster angle, as in Eq. (7). Ultrabroadband transmission is also confirmed in this scenario, even in the most mismatched case when a free-space input medium and glass output medium are considered. The vertical transmission band

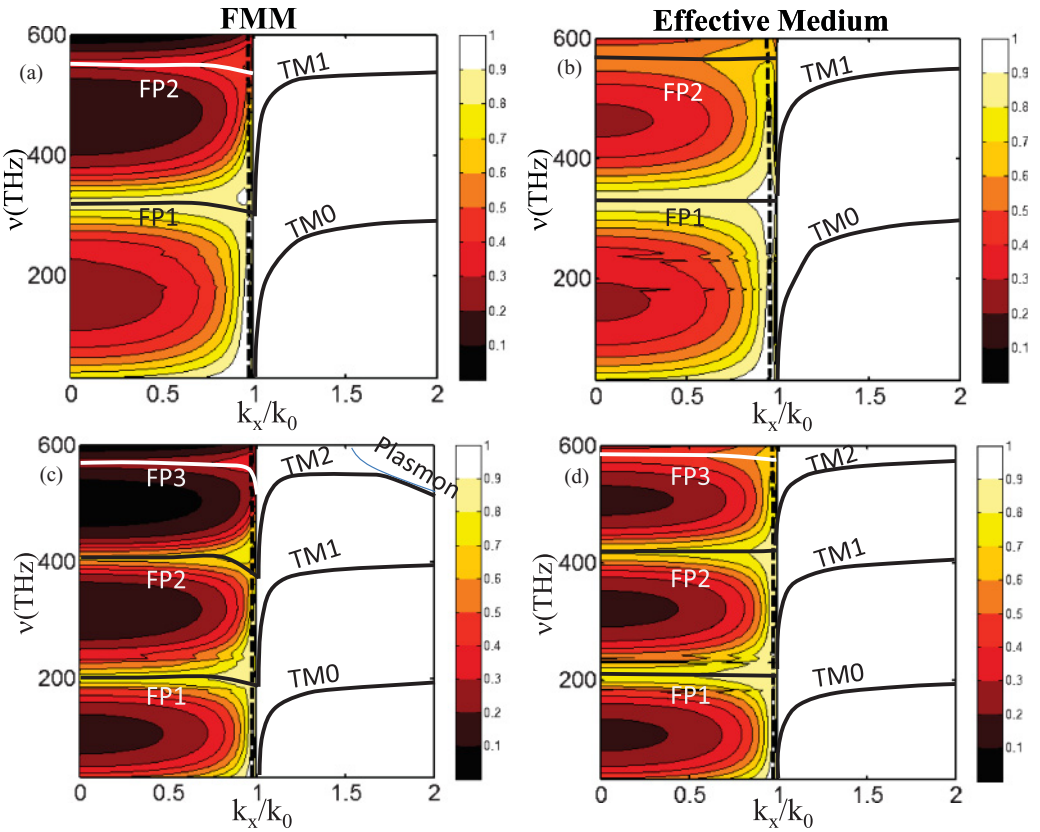

FIG. 6. (Color online) TM propagation and evanescent modes for two different grating designs: [(a),(b)] $w = 12$ nm, $d = 96$ nm, and $l = 200$ nm. [(c),(d)] $w = 24$ nm, $d = 192$ nm, and $l = 400$ nm. FMM-based simulations are shown in panels (a) and (c) and effective medium theory results are presented in panels (b) and (d).

is enhanced and moved to smaller angles when the input and output media are both composed of glass. The electromagnetic energy can tunnel more easily through the slits in this case, because their dimensions become electrically larger by a factor equal to the refractive index of glass. Figure 4 shows analogous results, but for a thicker screen $l = 400$ nm and a larger period $d = 192$ nm for a slit width $w = 24$ nm.

The horizontal FP transmission bands have narrower bandwidths and are more dense along the frequency spectrum, due to the longer slits. The anomalous impedance matching at the Brewster transmission, however, is not affected by the increased thickness of the structure, as predicted by Eq. (7). The transmission is slightly reduced at higher frequencies, due to the longer propagation path through the narrow slits, but absorption in the slits less affect the Brewster transmission than the conventional FP resonant mechanisms. This can be clearly seen in Fig. 5, which shows the absorption for two examples consistent with Fig. 4. Physically, this is associated to the significantly lower field enhancement within the slits compared to conventional plasmonic resonant tunneling. In general, the Brewster transmission is obtained over a broad frequency range from dc to the visible frequency around the specific angle θ_B independent of the grating thickness l. Indeed, our results show that it is possible to verify the Brewster tunneling phenomenon also in the presence of substrates and/or superstrates, which may also be used to tailor the angular spectrum of Brewster transmission, as indicated in Eq. (7).

III. EFFECTIVE MEDIUM ANALYSIS OF PLASMONIC BREWSTER DEVICES

Since the transmission-line model of the grating appears to describe with very good accuracy its complex interaction with the impinging wave, we have suggested in Ref. 11 that the grating may be modeled as an effective metamaterial, whose constitutive parameters satisfy

$$Z_{\text{eff}} = \sqrt{\frac{\mu_{\text{eff}}^{(s)}}{\varepsilon_{\text{eff}}^{(s)}}}\sqrt{1-\frac{\sin^2\theta}{\mu_{\text{eff}}^{(s)}\varepsilon_{\text{eff}}^{(s)}}} = \frac{w}{d}\frac{\beta_s}{k_0\varepsilon_w}. \tag{8}$$

To derive Eq. (8) we neglect the field penetration inside the metal, although we fully take into account its plasmonic properties and finite conductivity in the dispersion of β_s. By combining this equation with the requirement of momentum conservation for a homogeneous slab,

$$\varepsilon_{\text{eff}}^{(s)}\mu_{\text{eff}}^{(s)}k_0^2 = k_0^2\,\sin^2\,\theta + \beta_s^2, \tag{9}$$

we find that the plasmonic grating may be equivalently described as a homogeneous metamaterial slab with relative effective medium parameters:

$$\varepsilon_{\text{eff}}^{(s)} = (\varepsilon_w d)/w, \quad \mu_{\text{eff}}^{(s)} = w\left(\beta_s^2/k_0^2 + \sin^2\,\theta\right)/(\varepsilon_w d). \tag{10}$$

In this section, we discuss how the accuracy of this homogenization model is not limited to the Brewster condition, but it also extends in the evanescent part of the spectrum. In this way, we are able to connect the spectrum of guided modes supported by the grating, similar to a high-dielectric etalon, to the scattering resonances for propagating impinging waves. In Figs. 6(a) and 6(c), two gratings with different dimensions $w = 12$ nm, $d = 96$ nm, $l = 200$ nm and $w = 24$ nm, $d = 192$ nm, $l = 400$ nm and no material loaded in the slits ($\varepsilon_w = 1$), are simulated with the FMM technique. In the figure we show the dispersion of TM guided modes (solid lines) supported by the gratings, which clearly transition from the FP resonance branches ($k_x \leqslant k_0$) into the evanescent region ($k_x > k_0$). The modal dispersion has been calculated by using a rigorous procedure consisting in finding the zeros of the determinant of the scattering matrix in the (ν,k_x) plane. The Brewster angle condition is verified (dotted lines) as a vertical band, consistent with the previous discussion. Being a nonresonant phenomenon, this tunneling regime is not associated with any guided branch in the evanescent portion of the spectrum, as expected from the previous discussion.

Next, the grating is replaced with a homogeneous metamaterial slab with effective parameters (10). The transmission results are shown in Figs. 6(b) and 6(d) for the two previously mentioned gratings. The effective medium results agree well with simulations and predict both FP and Brewster transmission, as well as similar TM guided modes. Hence, the effective parameters are able to capture the response of the actual structure even in the evanescent region. This model holds as

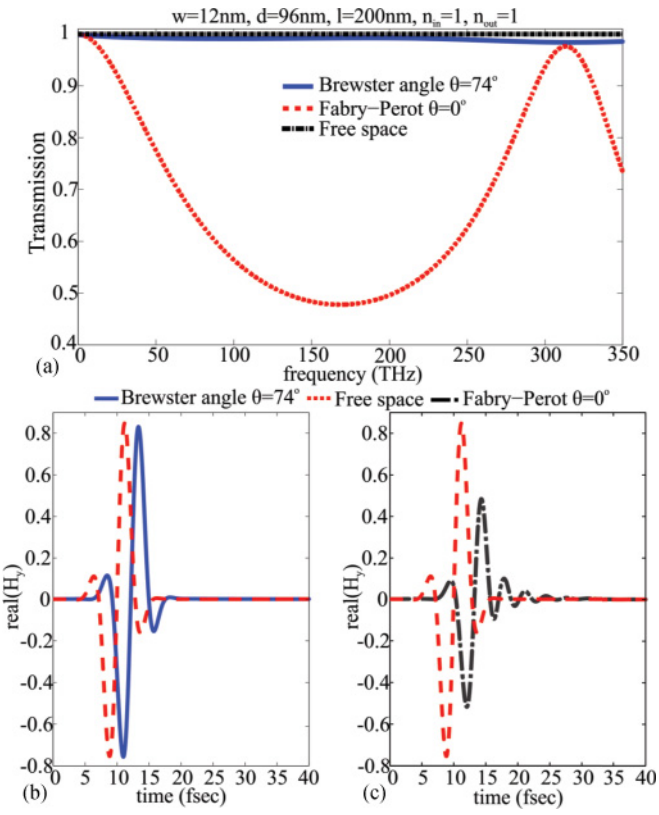

FIG. 7. (Color online) (a) Frequency response of the transmission coefficient through an optical grating with thickness $l = 200$ nm, period $d = 96$ nm, slit width $w = 12$ nm, and $\varepsilon_w = 1$. The surrounding background material is also free space. Time-domain response of the metallic grating illuminated by a short pulse (incident pulse is illustrated by the red dashed line) at (b) Brewster angle and (c) normal incidence.

long as there is no interaction with higher grating orders, as can be seen in the upper portion of Fig. 6(c). The accuracy of the model highlights the necessity to consider strong spatial dispersion effects in the metamaterial grating, associated with the propagation of slit modes that do not feel the transverse momentum of the impinging wave at oblique incidence. This is consistent with other metamaterial geometries consisting of elongated inclusions.[20,21]

IV. TIME-DOMAIN ANALYSIS OF PLASMONIC BREWSTER DEVICES ILLUMINATED BY ULTRASHORT PULSES

In this section, we explore the performance of plasmonic gratings illuminated at the Brewster angle condition by ultrashort pulses, using time-domain full-wave simulations. Due to the ultrabroadband performance of the funneling phenomenon described above, we expect that ultrashort pulses would tunnel almost completely undistorted through the grating. We consider first a grating with dimensions $w = 12$ nm, $d = 96$ nm, and $l = 200$ nm, with $\varepsilon_w = 1$, embedded in free space. The frequency and transient time-domain responses of this structure are shown in Fig. 7. We focus on a broad frequency window (0−350THz) to demonstrate the performance of the device, comparing excitation at normal incidence ($\theta = 0^\circ$) and at the plasmonic Brewster angle, which is approximately $\theta_B = 74^\circ$ for this example. The transmission coefficient is plotted against frequency in Fig. 7(a). Almost perfect transmission is obtained at the Brewster angle θ_B, as expected from the previous discussion. The performance is similar to free-space propagation, which is also shown in Fig. 7(a). On the contrary, FP resonances are dominant at normal incidence ($\theta = 0^\circ$) and high transmission is achieved only in a narrow range of frequencies. We launch an impulselike signal in time domain toward the grating at the two angles of incidence, with duration ∼10 fs, comparable with the bandwidth shown in Fig. 7(a).

The real parts of the transverse-magnetic component H_y of the transmitted pulse at the exit of the subwavelength corrugations are shown in Figs. 7(b) and 7(c) for the two incidence angles, compared to the pulse as obtained after free-space propagation. No distortions in time are obtained when the ultrashort pulse propagates at the Brewster angle θ_B. In contrast, the signal is distorted, reduced in amplitude, and spread in time for normal incidence, as expected. It should be noted that the signal transmitted at the Brewster angle, despite being transmitted without distortion, experiences a time delay compared to the free-space case, similar to ordinary propagation of a pulse through a dielectric slab, characterized by slower propagation. This is consistent with the analogy between the plasmonic grating and a dielectric slab outlined in Sec. III.

We also show similar plots for an optical grating with dimensions $w = 12$ nm, $d = 96$ nm, and $l = 200$ nm, when glass is placed at the exit of the structure $n_{\text{out}} = 1.52$. A mismatch is introduced at the outer boundary of the device, which does not severely affect its overall performance, as was shown in Fig. 3. The transmission coefficient for Brewster

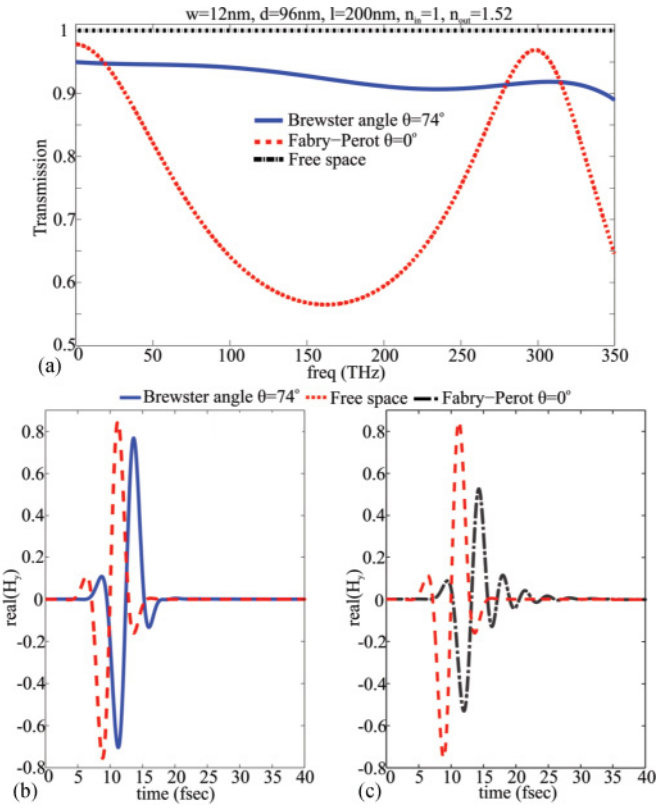

FIG. 8. (Color online) Similar to Fig. 7. The metallic grating is placed on a glass substrate with refractive index $n_{\text{out}} = 1.52$. The structure is mismatched at the outer boundary.

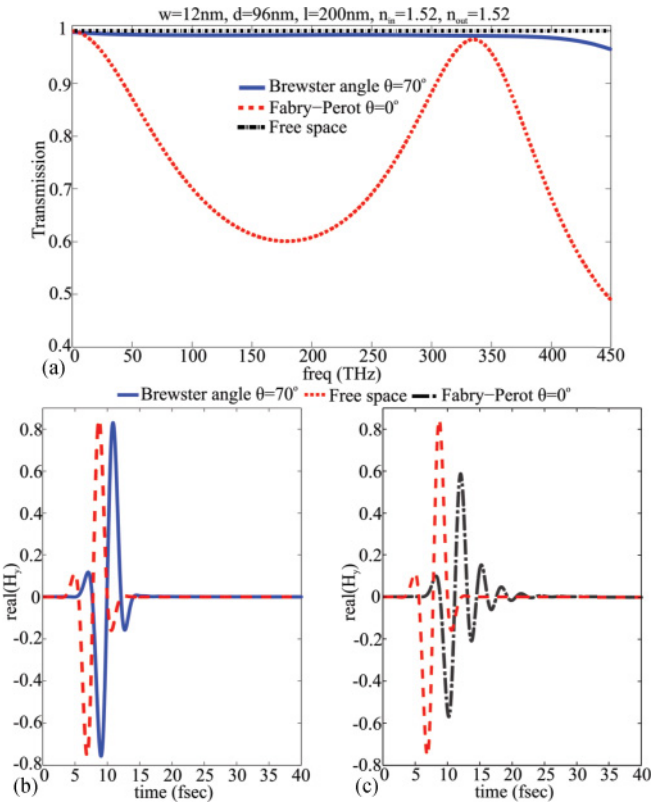

FIG. 9. (Color online) Similar to Fig. 7. The metallic grating is surrounded by glass background with $n_{\text{in}} = n_{\text{out}} = 1.52$.

incidence angle is shown in Fig. 8(a) and it is no longer identical to free space, due to the reflection at the second interface. However, it is still nearly uniform over a broad bandwidth (0−350 THz) compared with the normal incidence case, where narrow-band FP resonances are dominant. Again, an ultrashort pulse is launched at the two angles and the H_y components are monitored after the grating, shown in Figs. 8(b) and 8(c), respectively. It is seen that even in this mismatched case, due to the presence of a substrate, the short transmitted pulse is much less distorted at the plasmonic Brewster angle. It is envisioned that in a future experimental demonstration of the optical grating, it will be easier to place the slit array on a glass substrate, similar to the present example, without severely impairing the broadband funneling effect.

Finally, the transient response of the optical grating is explored for similar dimensions $w = 12$ nm, $d = 96$ nm, and $l = 200$ nm surrounded by glass background on both sides ($n_{\text{in}} = n_{\text{out}} = 1.52$). The uniform flat transmission coefficient now extends until 450 THz at the Brewster condition, as shown in Fig. 9(a). Hence, even better ultrabroadband performance is achieved for this case compared to the free-space background considered in Fig. 7(a) because the effective electrical slit width becomes larger when considering a dielectric superstrate/substrate. In this case, the Brewster angle shifts to $\theta_B = 70^\circ$, smaller than the previous cases ($\theta_B = 74^\circ$), as predicted by Eq. (7). The transient response of a transmitted ultrashort pulse for Brewster and normal incidence is shown in Figs. 9(b) and 9(c). Again, the impulse is transmitted with minimal distortions at the Brewster angle, compared with the spread in time obtained at normal incidence. By including a matched superstrate, we are able to achieve even more exciting funneling performance for ultrashort pulses and get additional degrees of freedom in tuning the bandwidth, beamwidth, and angular performance of the device.

V. CONCLUSIONS

We have considered here the implications of the Brewster funneling for plasmonic gratings in various optical setups, extending our results in Ref. 11. We have considered a semi-infinite interface to mimic the situation in which the impinging energy is absorbed in the grating, and the influence of substrate and superstrate materials. Ultrabroadband EOT, spanning from zero frequencies (dc) to the breakdown of the TL model ($d \simeq 0.5\lambda_0$, where d is the period and λ_0 is the wavelength in free space or in the substrate/superstrate) for an otherwise opaque metallic grating slab, has been verified both in frequency and time domain, showing its functionality in the case of ultrashort pulses. Finally, the effective medium equivalent of the plasmonic grating was found to accurately predict its behavior for propagating and evanescent modes. The proposed tunneling mechanism is the physical analog of the well-known Brewster angle condition in optics for TM oblique incidence waves on dielectric etalons, but it is now obtained in ultranarrow slits, creating large, broadband energy concentration of interest in a variety of applications, spanning energy harvesting, emission, and polarization filtering. We are planning to extend this interesting concept to two-dimensional structures in our future work.

ACKNOWLEDGMENTS

This work has been partially supported by ARO with STTR W31P4Q-09-C-0652, by the AFOSR YIP award No. FA9550-11-1-0009, and by an ONR MURI No. N00014-10-1-0942.

*alu@mail.utexas.edu

[1] T. W. Ebbesen, H. J. Lezec, H. F. Ghaemi, T. Thio, and P. A. Wolff, Nature (London) **391**, 667 (1998).
[2] F. J. García de Abajo, Rev. Mod. Phys. **79**, 1267 (2007).
[3] F. J. Garcia-Vidal, L. Martin-Moreno, T. W. Ebbesen, and L. Kuipers, Rev. Mod. Phys. **82**, 729 (2010).
[4] J. B. Pendry, L. Martín-Moreno, and F. J. García-Vidal, Science **305**, 847 (2004).
[5] X. R. Huang, R. W. Peng, and R. H. Fan, Phys. Rev. Lett. **105**, 243901 (2010).
[6] L. B. Mashev, E. Popov, and E. G. Loewen, Appl. Opt. **28**, 2538 (1989).
[7] J. A. Porto, F. J. García-Vidal, and J. B. Pendry, Phys. Rev. Lett. **83**, 2845 (1999).
[8] P. Lalanne, J. P. Hugonin, S. Astilean, M. Palamaru, and K. D. Moller, J. Opt. A, Pure Appl. Opt. **2**, 48 (2000).
[9] E. Popov, S. Enoch, and N. Bonod, Opt. Express **17**, 6770 (2009).
[10] F. Pardo, P. Bouchon, R. Haïdar, and J.-L. Pelouard, Phys. Rev. Lett. **107**, 093902 (2011).
[11] A. Alù, G. D'Aguanno, N. Mattiucci, and M. J. Bloemer, Phys. Rev. Lett. **106**, 123902 (2011).
[12] G. Subramania, S. Foteinopoulou, and I. Brener, Phys. Rev. Lett. **107**, 163902 (2011).
[13] Z. Wang, G. Li, F. Xiao, F. Lu, K. Li, and A. Xu, Opt. Lett. **36**, 4584 (2011).
[14] Y. Sun, B. Edwards, A. Alù, and N. Engheta, Nat. Mat. (to be published).
[15] F. Medina, F. Mesa, and R. Marques, IEEE Trans. Microwave Theory Tech. **56**, 3108 (2008).
[16] A. Fernandez-Prieto, F. Medina, and F. Mesa, Appl. Phys. Lett. **95**, 021108 (2009).
[17] A. Alù and N. Engheta, J. Opt. Soc. Am. B **23**, 571 (2006).
[18] L. Li, J. Opt. Soc. Am. A **13**, 1870 (1996), and references therein.
[19] E. D. Palik, *Handbook of Optical Constants of Solids* (Academic, New York, 1991).
[20] W. Rotman, IRE Trans. Antennas Propag. **10**, 82 (1962).
[21] P. A. Belov, R. Marqués, S. I. Maslovski, I. S. Nefedov, M. Silveirinha, C. R. Simovski, and S. A. Tretyakov, Phys. Rev. B **67** 113103 (2003).